Cent. Eur. J. Phys. • 10(2) • 2012 • 459-469
DOI: 10.2478/s11534-011-0108-2

VERSITA

Central European Journal of **Physics**

Asymmetric double quantum wells with smoothed interfaces

Research Article

Vladimir Gavryushin[1]*

1 *Institute of Applied Research and Semiconductor Physics department, Vilnius University, Sauletekio al. 9-III, 10222 Vilnius, Lithuania*

Received 26 August 2011; accepted 16 November 2011

Abstract: We have derived and analyzed the wavefunctions and energy states for an asymmetric double quantum well (ADQW), broadened due to interdiffusion or other static interface disorder effects, within a known discreet variable representative approach for solving the one-dimensional Schrodinger equation. The main advantage of this approach is that it yields the energy eigenvalues, and the eigenvectors, in semiconductor nanostructures of different shapes as well as the strengths of the optical transitions between them. The behaviour of ADQW states for the different mutual widths of coupled wells, for the different degree of broadening, and under increasing external electric field is investigated. We have found that interface broadening effects change and shift energy levels, not monotonously, but the resonant conditions near an energy of sub-band coupling regions do not strongly distort. Also , it is shown that an external electric field may help to achieve resonant conditions for inter-sub-band inverse population by intrawell emission of LO-phonons in diffuse ADQW.

PACS (2008): 73.21.Ac, 73.63.Hs

Keywords: multi-barrier quantum well structures • asymmetric double quantum wells • quasi-bound levels • discreet variable representation • Schrodinger equation

© *Versita Sp. z o.o.*

1. Introduction

When a thin (~100 A layers of one semiconductor (e.g. GaAs) are sandwiched between layers of another semiconductor with a larger band gap (e.g. AlGaAs), carriers are trapped and confined in two dimensions (2D), due to the potential barriers. As a result of quantum confinement, discrete energy states (or "sub-bands") occur, which change dramatically electronic and optical properties of such structures, known as the quantum wells (QWs). When the quantum wells are coupled there exist probabilities for the electron tunnel, which can be in either of the two wells. The novel optical properties of the 2D electron gas appear associated with the transitions between quantized sub-bands, so called "inter-sub-band transitions", which correspond to the range from mid-infrared to terahertz (THz) photon energies. They have narrow line-widths and extremely large dipole moments of transitions.

In recent years, there has been considerable interest in asymmetrical multiple-quantum well systems [1], because many new optical devices based on inter-sub-band tran-

*E-mail: v.gavriusinas@cablenet.lt

Springer

sitions are being developed ("inter-sub-band optoelectronics" [2]). This feature could fulfill the need for efficient sources of coherent infrared (IR) radiation for several applications, such as communications, radar, and optoelectronics. Their most spectacular applications are quantum well IR photodetectors [3] and the quantum cascade (QC) lasers [4], that relies on the cascaded inter-sub-band transitions and resonant tunneling between adjacent QWs. These devices are made with epitaxially grown GaAs/AlGaAs, InGaAs/AlInAs, GaN/AlGaN [1, 5]], and Si/SiGe [6] systems. With the recent development on semiconductor device growth technology, multi-barrier quantum well structures are becoming the basic building blocks of modern semiconductor devices, such as resonant tunneling diodes (RTD) [7], high-speed light modulators [8, 9], wavelength tunable lasers [10, 11], far-infrared and THz lasers [12], quantum cascade (QC) lasers [4, 13], *etc*.

In an inter-sub-band quantum cascade laser, the population inversion must be established by engineering the lifetimes and oscillator strengths, *i.e.* by a suitable design of the active region. Calculations for quantum wells are often performed in the approximation where the conduction and valence band offsets are taken as sharp step functions. In practice, real QW structures tend to deviate from the ideal homogeneous heterostructures with perfect abrupt interfaces due to the fluctuations of the band edges (Fig. 1), and inter-diffusion which thus is not very well defined. The reasons for this are the stochastic processes of the crystal growth leading to local variations of chemical composition, well width, and lattice imperfections to name a few. Since a QW is generally a heterostructure formed by a binary semiconductor (AB) and a ternary disordered alloy ($AB_{1-x}C_x$), as in GaAs/InGaAs, there are two types of disorders responsible for the inhomogeneous broadening: compositional disorder, caused by concentration fluctuations in a ternary component, and random diffusion across the interface.

Surface segregation during epitaxial growth [14] and thermal annealing [15] processes may result in the symmetric inter-diffusion at interfaces [15]. Both processes change the electronic behaviour of a system by narrowing the QWs and degrading the barriers of QWs. In such *inter-diffused* or *inter-mixed* QW structures with smooth interface profiles, significant changes in the sub-band spacing and carrier scattering rates in a Si/SiGe QW system [6], were predicted.

The inter-diffused QW structures such as GaAs/AlGaAs [16] and InP/InGaAs [17, 18] have been actively investigated for improved inter-sub-band electro-absorptive light modulation [17, 18], and widely used in several optical devices, such as electro-absorptive [19] and lateral confinement [20] waveguides, light modulators [21, 22], and wavelength tunable lasers [10, 11]. The improved quantum confinement and a higher tunneling rate achieved in the inter-diffused QW's cannot be fulfilled by a rectangular QW structure simultaneously. The extensively inter-diffused QW reduces the required bias or increases the tunneling rate for EA modulation. Therefore, the diffused QW structure is potentially attractive for developing high-speed modulators. The effect of inter-diffusion has been simulated and investigated below.

The genius of the QW heterostructure concept—and the quantum cascade in particular—lies in its innate engineerability. In order to design new devices or optimize the device performance, and thus properly predict their behavior, one needs to know the detailed information of quasi-bound levels in real disordered multi-barrier quantum well structures. Theoretical studies of the influence of the compositional and interface disorder on the motion of free carriers in nanostructures have a long history [23–25]. There have been calculations for phenomena like exciton localization at lateral fluctuations of the well width and band tails [26, 27] as shown in Fig. 1c due to fluctuations in impurity concentration.

To understand the physical properties of the heterostructure devices, one needs to solve the eigenvalue problem of carriers in QWs. It is well known that exact analytical solutions to such problems are only available for simple structures such as a square or parabolic well [28], and even in these structures, in general, in the presence of perturbations such as external fields, disorder effects [29], *etc*., the problem cannot be solved exactly. There have been various numerical methods used to calculate the band profiles in QWs: the matrix approach (MA) [30, 31], the transfer matrix (TM) method [32, 33], the finite difference method (FDM) [34, 35], the "shooting method" (SM) [34, 36], the finite element (FE) technique [37, 38], discreet variable representation (DVR) approach [39], envelope function (EF) method [40], Wentzel–Kramers–Brillouin (WKB) approximation [41], variational method (VM) [42], and Monte Carlo (MC) simulations [43]. Among them, the WKB and EF methods adopt approximations, thus giving unreliable results; the VM only works well at simple QWs and weak fields; the MC and FE methods are highly computer-orientated approaches; the MA usually require wave function to be well behaved; the SM's speed comes at the cost of stability. The DVR and TM methods overcome all the shortcomings listed above and could be easily applied to any potential profiles of biased/unbiased multi-barrier quantum well structures.

In this paper, we describe a numerical technique based on the DVR approach, as a grid-point representation (grid discretisation method) of a Hamiltonian matrix element [29, 39, 44] which is capable of solving the eigenvalue and

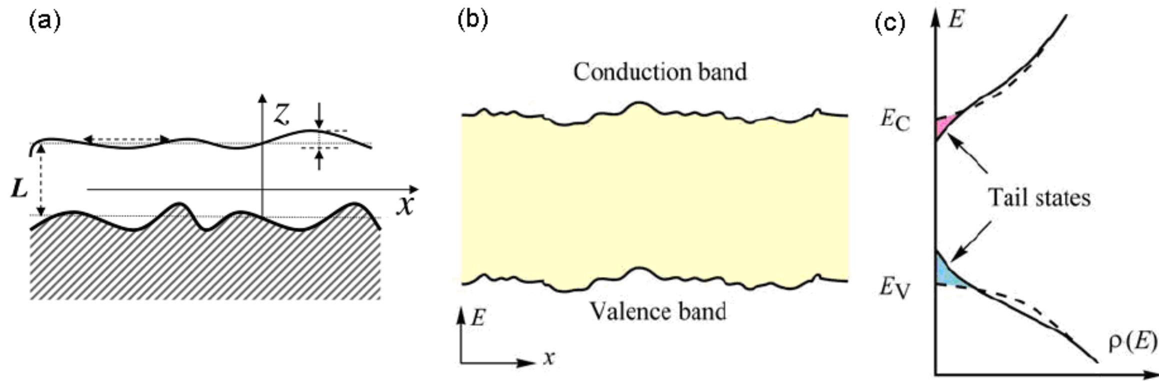

Figure 1. a) Characteristic length scales describing the interface roughness of a QW. (b) Spatially locally fluctuating band edges caused by random distribution of impurities [46]. (c) Resulting densities of states in the conduction with tail states extending into the forbidden gap. The dashed lines show the parabolic densities of states in undoped semiconductors.

eigenfunction problems in an arbitrary QW under arbitrary perturbation. Calculation results for energy levels and wave functions of an asymmetric double quantum well with sharp interfaces and inter-diffused interfaces with gradual variation of the potential, are presented and compared.

2. Calculation details

2.1. A model of the interface disorder effects

Randomly distributed charged dopants, or composition x in mixed crystals A_xB_{1-x}, lead to unavoidable fluctuations of the doping impurities concentration on a microscopic scale. Semiconductor heterostructures possess a certain degree of disorder due to their alloy structure and/or imperfect interfaces. Two things influence interface disorder effects: coordinate fluctuations of interface position (Fig 1a), and gap energy $E_g(x)$ fluctuations (Fig. 1b,c) due to the randomly distributed dopants. These fluctuations result in potential fluctuations giving rise to band tails composed from localized states. This situation is schematically shown in Fig. 1. The magnitude of band-edge energy fluctuations (Fig. 1b,c) caused by the random distribution of charged donors and acceptors was first calculated by Kane [45]. States with energy below the unperturbed conduction band edge or above the unperturbed valence band edge are called tail states, which significantly change the density of states in the vicinity of the band edge.

Particularly simple 1D models of an electron moving in a random or diffused potential are possible. If the fluctuations are not too large, good approximation is obtained by calculating spectra for slightly different configurations and adding them up using some broadening weight factor.

Inhomogeneous broadening, due to site variation produced by a random distribution of local crystal fields, results in a Gaussian type broadening [45]. Homogeneous broadening, from dynamic perturbations on energy levels and equally on all ions, leads to a Lorentzian type broadening. So, a QW's barrier interface roughness may be approximated [29] by the *convolution* of Heaviside step function $\Phi(x-x_0)$ with an area normalized, a moving Gaussian broadening envelope function of width σ_G [45]:

$$H_G(z,z_0,\sigma)=\frac{1}{\sqrt{2\pi}\sigma_G}\int_0^{\infty}\exp\left[-\frac{(z-x)^2}{2\sigma_G^2}\right]\Phi(x-z_0)dx, \tag{1}$$

or with the Lorentzian broadening envelope function of width Γ:

$$H_L(z,z_0,\Gamma)=\frac{\Gamma}{\pi}\int_0^{\infty}\frac{1}{(z-x)^2+\Gamma^2}\Phi(x-z_0)dx. \tag{2}$$

A convolution (smoothing) procedure [47] is an integral that expresses the amount of overlap of envelope function (*i.e.* Gaussian or Lorentzian) as it is shifted over another function Φ. Instead of the ∞ limit usually used in integration, we take any value big enough for the resultant convergence.

The barrier steps may also be broadened in an extremely simple analytical way, - by applying of the phenomenological atan(x) function against the Heaviside step function $\Phi(x)$, usual for an ideal heterostructure with perfect interfaces:

$$\Phi(z-z_i)\Rightarrow\frac{\pi}{2}+\arctan\frac{z-z_i}{\Gamma_i}, \tag{3}$$

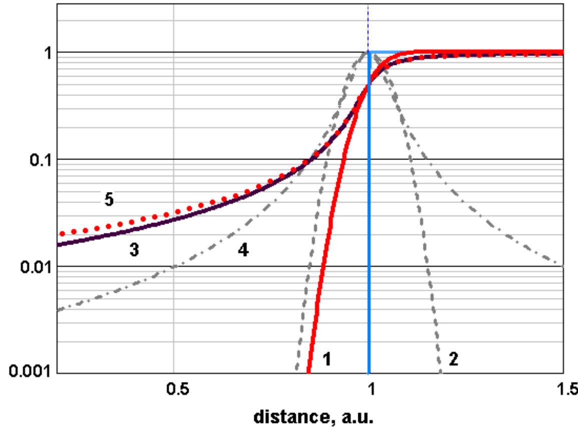

Figure 2. Comparison of convolution broadenings of the Heaviside step-function with different broadening functions: 1 – Gaussian broadened step; 2 – Gaussian envelope; 3 – Lorentzian broadened step; 4 - Lorentzian envelope; 5 – Analytical arctan(x) approximation curve (3); Analytical error function profile (4) is fully overlapped with curve 1. Broadening parameter Γ = 0.05 nm.

where Γ_i is the broadening parameter of the interfaces at z_i. This function with zero mean z_i, characterises the deviation of the ith interface from its average position. The inter-diffusion of the QW composition profile is described, usually, by an error function erf(x) [6, 15, 48]:

$$\Phi(z-z_i) \Rightarrow \frac{1}{2}\left[1+erf\left(\frac{z-z_i}{\sqrt{2}L_d}\right)\right]. \quad (4)$$

The extent of the inter-diffusion process is characterised by a diffusion length L_d. Examples of calculated functions (1)-(4) are presented in Figure 2. An analytical error function profile (4) is fully overlapped with the Gaussian broadened step (curve 1). As we see in Figure 2, function (3) (red dots) may be a good approximation for convolution of Heaviside function by Lorentzian envelope (2) (curve 3). To our knowledge, any attempts to use the Lorentzian type broadening or interdiffusion modeling have been published, so annealed QW interfaces were simulated below in such a kind.

2.2. Method of discrete variable representation (DVR)

Analytical solutions for asymmetrical double and triple quantum-wells are possible only for unbiased sharp rectangular QWs [49]. We select discrete variable representation (DVR) as a numerical method [39, 50] for our MathCAD calculations of a stationary 1D Schrodinger equation for confined eigenstates. Different types of DVR methods have found wide applications in different fields of problems [51, 52]. We also carried out DVR calculations for QWs and unharmonic Morse potential [29, 44].

The DVR is a numerical grid-point method in which the matrix elements of the local potential energy operator V(r) is approximated as a diagonal matrix (mnemonic: DVR - **d**iagonal **V**(**r**), or **D**iscrete **V**ariable **R**epresentation): $V_{ik} = \langle\phi_i|V|\phi_k\rangle = \delta_{ik}V(x_i)$ [53], and the kinetic energy matrix is full, but it has a simple analytic form, as a sum of 1D matrices. DVR method is selected since it avoids having to evaluate integrals in order to obtain the Hamiltonian matrix and since an energy truncation procedure allows the DVR grid points to be adapted naturally to the shape of any given potential energy surface. The DVR method greatly simplifies the evaluation of Hamiltonian matrix elements $H_{ik} = \langle\phi_i|H|\phi_k\rangle$ and obtains the eigenstates and eigenvalues by using standard numerical diagonalization methods of MathCAD or Mathematica.

If we choose an equally spaced grid, $x_i = i\Delta x$, ($i = 0, \pm1, \pm2, ... \pm N$), then the DVR gives an extremely simple grid-point representation of the kinetic energy matrix $\hat{T}_{i,k} = \hbar^2 k_{i,k}^2/2m^*$ within the conditional formulation [39]:

$$\hat{T}_{i,k} = g\begin{Bmatrix} \pi^2/3, & i=k \\ \frac{2(-1)^{i-k}}{(i-k)^2}, & i\neq k\end{Bmatrix}. \quad (5)$$

The only parameter involved being the grid spacing Δx via an energetically weighted grid parameter g (“energy quantum of the grid”):

$$g = \frac{\hbar^2}{2m^*}\left(\frac{1}{\Delta x}\right)^2, \quad (6)$$

where m^* is the electron effective mass. So, if the grid points are uniformly spaced then numerical solutions of a matrices elements of the full energy Hamiltonian operator

$$\hat{H} = \hat{T} + \hat{V} = -\frac{\hbar^2}{2m^*}\frac{d^2}{dx^2} + V(x)$$

is as [39]:

$$\hat{H}_{i,k} = \hat{T}_{i,k} + \hat{V}_{i,k} = \frac{\hbar^2}{2m(\Delta x)^2}(-1)^{i-k}\times$$

$$\times\left(\frac{\pi^2}{3}\delta_{i,k} + \frac{2}{(i-k)^2}(1-\delta_{i,k})\right) + V(x_i)\,\delta_{i,k} \quad (7)$$

when the δ-functions are placed on a grid that extends over the interval x = (-∞,∞). First term in parenthesis is a value of second term in the limit $N\to\infty$ [39].

In our calculations the potentials of an ideal and of a broadened biased/unbiased double QW are used as [29]:

$$V_1(x_i) = U_1\left[1+\Phi(x_i-R_1)-\Phi(x_i)\right] + V_{bias}(x_i),$$

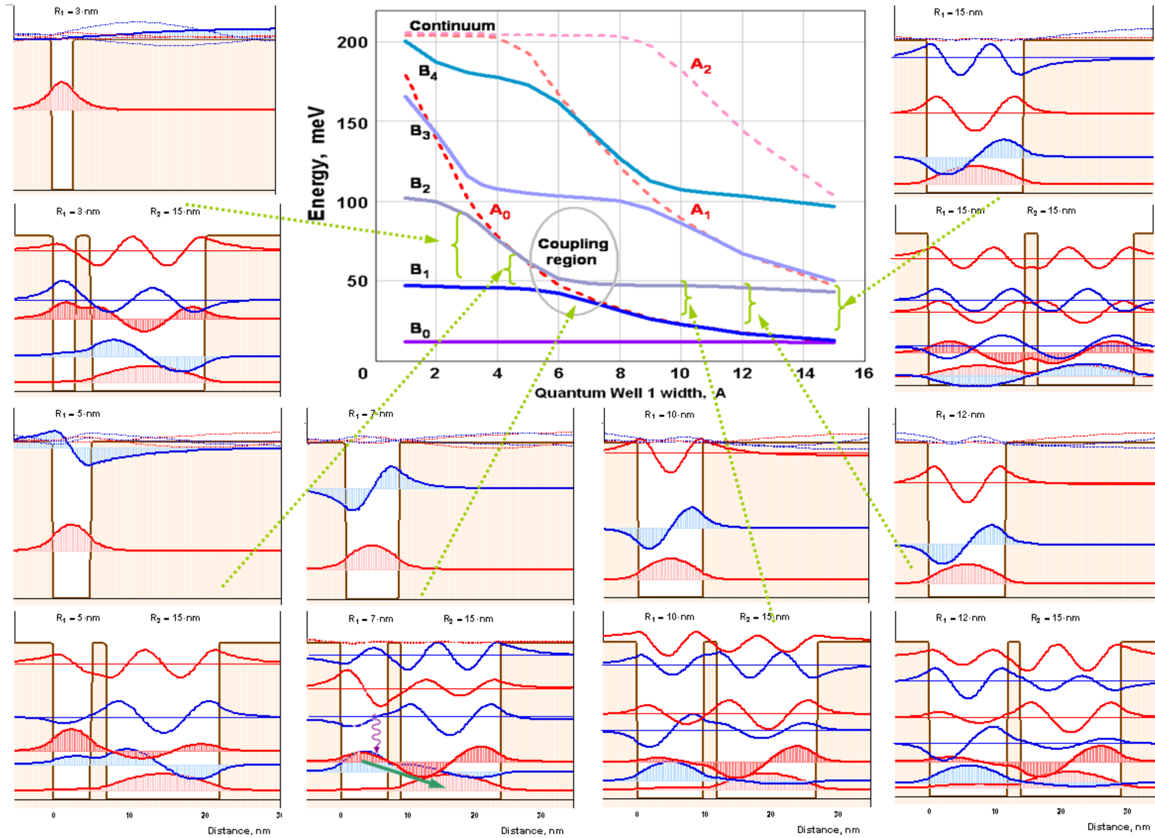

Figure 3. Unbroadened ideal ADQWs case. Dependencies of the positions of the five lowest subbands $B_0 - B_4$ (in eV) as a function of the narrower well width R_1 (= 3, 5, 7, 10, 12, 15 nm) for fixed values R_b = 2 nm and R_2 = 15 nm. Broken lines are the same dependencies of the A states for a single quantum well of R_1 width. The insets around show the model band diagrams with energy levels and corresponding wavefunctions of an asymmetric double quantum well heterostructures. The wavy arrow indicates the stimulating light-emitting transition, assisted by the fast resonant optical-phonon emission (arrow between states $n = 1$ and $n = 0$) in the heterostructure. Calculated region: -30 nm ÷ +30 nm with 500 grids.

$$V_2(x_i) = V_1(x_i) + U_2 \times$$
$$\times [-\Phi(x_i - R_b - R_1) + \Phi(x_i - R_b - R_1 - R_2)], \quad (8)$$

and

$$V_1(x_i) = U_1 \left[1 + \frac{1}{\pi} a \tan\left(\frac{x_i - R_1}{\Gamma}\right) - \frac{1}{\pi} a \tan\left(\frac{x_i}{\Gamma}\right) \right] + V_{bias}(x_i),$$

$$V_2(x_i) = V_1(x_i) + U_2 \left[-\frac{1}{\pi} a \tan\left(\frac{x_i - R_b - R_1}{\Gamma}\right) - \frac{1}{\pi} a \tan\left(\frac{x_i - R_b - R_1 - R_2}{\Gamma}\right) \right], \quad (9)$$

correspondingly. Here $\Phi(x)$ is a Heaviside step function; $U_{1(2)}$ are the depths of potential wells (differences in the offset band energies) for the 1st and 2nd QW of the widths $R_{1(2)}$; and R_b is the barrier width. The applied bias potential here

$$V_{bias}(x_i) = \begin{vmatrix} V_{cont}, & \text{if} \quad x_i < R_{cont} \\ E_f \cdot x_i, & \text{otherwise} \end{vmatrix} \quad (10)$$

$$V_{cont} = U_1 [1 - \Phi(R_1 - R_{cont}) + \Phi(R_{cont})] + E_f \cdot R_{cont},$$

is used when an electric field E_f perpendicular to the quantum well is applied in calculations.

3. Results and discussion

Inter-well optical-phonon-assisted transitions are studied in an asymmetric double-quantum-well heterostructures [53] comprising one narrow and one wide coupled quantum wells (QWs). It is shown that the depopulation rate of the lower sub-band states in the narrow QW can be significantly enhanced thus facilitating the inter-sub-band inverse population, if the depopulated sub-band is aligned

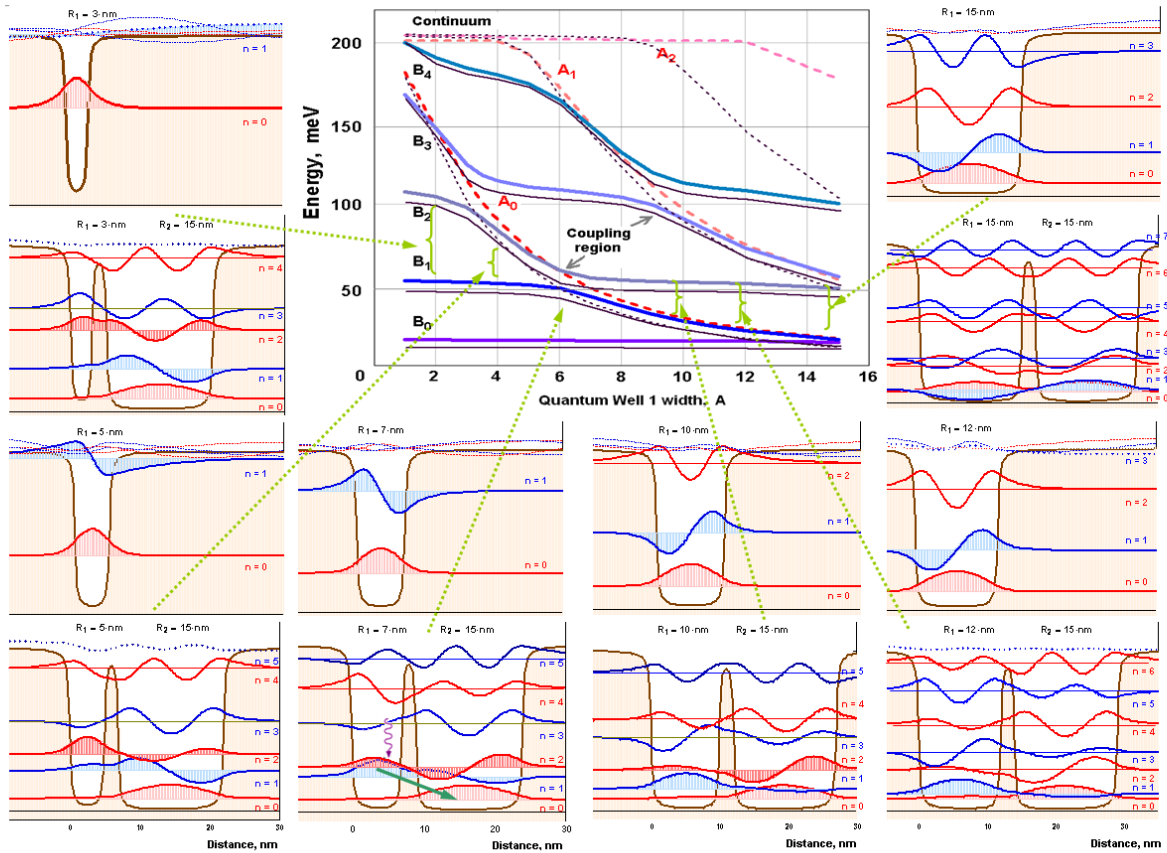

Figure 4. Broadened ADQWs with interdiffused interfaces. Dependencies of the positions of the five lowest sub-bands B_0 – B_4 (in eV) as a function of the narrower well width R_1 (= 3, 5, 7, 10, 12, 15 nm) for fixed values R_b = 2 nm and R_2 = 15 nm. Broken lines are the same dependencies of the three A_i states for a single QW with the width R_1. For comparison, thin black lines presents the case of ideally rectangle shaped ADQWs as in Fig. 3. The insets around shows the model band diagrams with energy levels and corresponding wavefunctions. Interface roughness parameter Γ = 0.2 nm. Calculated region: -30 nm ÷ +30 nm with 500 grids.

with the second sub-band of the wider QW, while the energy separation from the first sub-band is tuned to the energy of optical phonon mode. Such mentioned structure under applied bias is working as a "resonant-phonon type" active region of stimulated emission in the far-infrared quantum cascade lasers (QCL) [54]. Laser operation [4] is based on stimulated radiative transitions between inverse populated states (wavy arrows at Fig. 7a). Depopulation of lower state is achieved by setting the sub-band separation between 1st and 2nd levels to the LO-phonon resonance energy, which causes electrons to quickly relax from level 2 via electron-phonon scattering (bold arrow at Fig. 7a). An overview of QCL physics, including development and applications, are given in the review papers [55, 56].

Seeking to reproduce mentioned effects, the eigenvalues (stationary energy states E_n) and the eigenvectors (wavefunctions ψ_n) for a quantum number n, as the solutions of the Schrodinger equation $\hat{H}\psi_n(r) = E_n\psi_n(r)$, were calculated using standard numerical diagonalization methods (eigenvals(H) and eigenvec(H) commands in MathCAD) for the DVR Hamiltonian (7).

Results of our DVR calculations of such a laser structure, as in [53], are depicted in Fig. 3 as the eigenstates, together with the corresponding wavefunctions, for the coupled asymmetric square quantum wells with the potentials of the form (8). The states over the dissociation energy U are unbound and delocalised. Dependencies of the positions of the five lowest sub-bands B_i as a function of the narrow well width values R_1 = 3, 5, 7, 10, 12, 15 nm for the fixed values of barrier width R_b = 2 nm and of the second QW width R_2 = 15 nm are shown in Fig. 3. Broken lines are the same dependencies for the A_i states of a 1st, but single, quantum well with the same width R_1. Comparing the fans of dependencies for A_i and B_i states for single and double QW's, we can resolve the doublet nature of the states and especial coupling (anti-crossing) regions of the levels in double QW. The insets

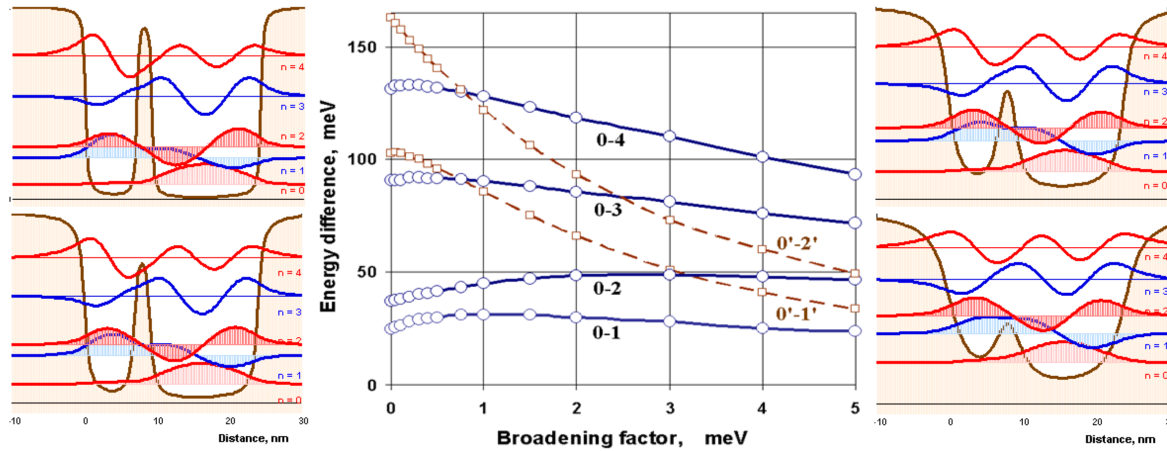

Figure 5. Conduction band potential, confined electron states and wavefunctions shown schematically for varying degrees of interdiffusion [Γ = 0.2, 0.5, 1, and 2 nm] for ADQW, same as in Figure 4. Left QWs width is R_1 = 7 nm; right QWs width is R_2 = 15 nm; barrier width is 2 nm. Middle fan represents the subband spacing as a function of broadening factor Γ.

around in Fig. 3 show the model band diagrams with energy levels and corresponding wavefunctions of an ADQW heterostructures (AlGaAs/GaAs).

It is useful also to have some indication of how many grid points are necessary for this DVR procedure to provide an accurate description of a quantum system. Convergence of the calculation can be checked by decreasing the number of grid used in the calculation. For full convergence of the calculation results, we found that a big enough grid number is $N \geq 50$, however we have used the number of calculus points $N = 500$ for the better shaping of calculated wavefunctions.

All states in double QWs are split doublets, because the degeneracy is unmounted by different parity properties. When the barrier thickness becomes smaller, quantum coupling due to the tunneling between the wells is dominant. As a consequence, an energy splitting (anticrossing) occurs (coupling regions indicated in Fig. 3 and Fig. 4) and the respective electron states, the so-called binding (symmetric) and anti-binding (antisymmetric) states, are delocalised over both wells. The minimum energy splitting or tunnel coupling ΔE (anticrossing gap) is determined by the barrier thickness R_b and height. The lowest coupled state is mainly localised in the wide well and the other state is mainly localised in the narrow well. Due to the coupling of the two wells the two states have nonzero probability density in both wells.

One embodiment of THz laser structure is depicted in Fig. 3 and Fig. 4 where the energy levels in coupling region are separated by energy equal to the optical phonon energy. The wavy arrow corresponds to the stimulated light-emitting transition, assisted by the fast resonant optical-phonon emission (arrow between states $n = 1$ and $n = 0$). Phonon-assisted transitions between the coupled levels depend strongly on the phonon energy involved in the transition.

Even with the sophisticated growth technologies used in current structures, the presence of interface and alloy disorder induces noticeable effects. The results of DVR calculations of the same family of ADQWs as in Fig. 3, but with broadened interfaces with the potentials approximated by (9), using interface smoothing $\Gamma = 0.2$ nm, are depicted in Fig. 4. In the central part of Fig. 4, for comparison, both energy fans for ideal rectangular interfaces (as in Fig. 3), and for broadened ones, are presented together. Here the thin black lines represent the case of sharp rectangular shaped ADQWs. As we see, interface broadening changes shift energy levels to the higher energies, but the resonant conditions near an energy coupling region are not strongly distorted. The blue shift is as a sequence of an effective narrowing of the distorted QWs, and the changes seen in the coupling regions are caused from the different inter-well barrier profile.

Such modest one-dimensional modeling results for QWs may correspond to the mean effects from the lateral fluctuations in the plane of QWs. Interface roughness as 3D problem affects in general the dynamics of confined exciton states [26, 27] or scattering processes [57]. The ambiguity is due to the continuous spatial variation of interface from alloy composition. It is usually assumed that the 3D interface roughness parameters are independent of interdiffusion. In reality, however, annealing-like diffusion processes may reduce the interface roughness height.

Similar calculations, but for a single heterojunction with transition layer, were performed in [58], where also was shown that interface smoothing gave small effects to the

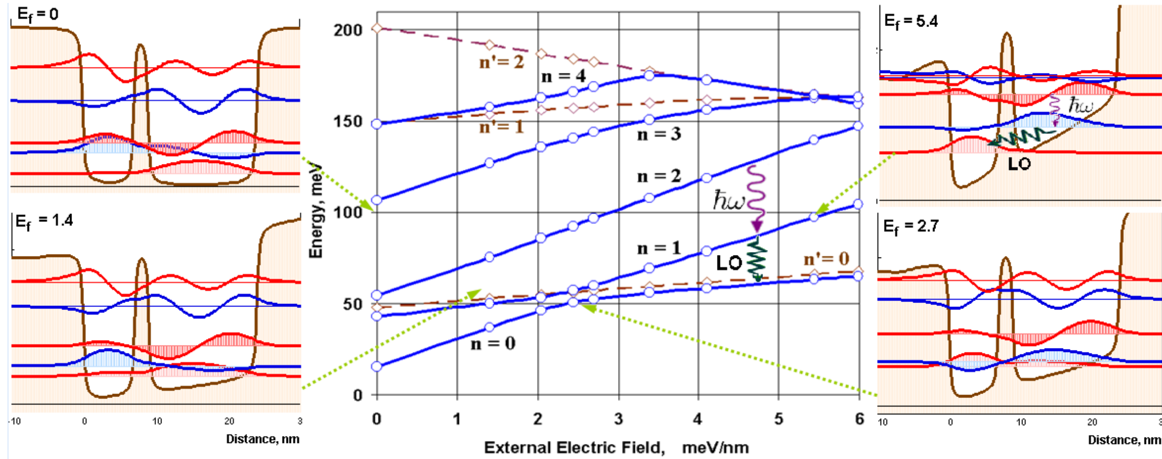

Figure 6. Confined electron states and wavefunctions dependence on an electric field [$E = 0, 1.4, 2.7, 5.4$ meV/nm] applied perpendicular to the diffused (Γ = 0.2 nm) ADQW layer plane, same as in Figure 4. Left QW width R_1 = 7 nm; right QW width R_2 = 15 nm; barrier width is 2 nm. Zero external field, or metal contact position R_{cont} is selected at -7 nm.

energy level differences, - they are relatively insensitive to the interface profile. Inter-sub-band carrier scattering in Si/SiGe quantum wells with diffuse interfaces was investigated in [6].

3.1. Effect of the Interdiffusion degree to the states of ADQW

To estimate the effect of inter-diffusion upon barrier degradation [6], same pairs of QWs separated by a thin barrier were considered. Figure 5 shows the results for the coupled diffuse double quantum well, resolving the effect of inter-diffusion degree Γ on the sub-band spacing $\Delta E_{nn'}$. As the broadening factor Γ increases, the bottom of the wells narrow and the top widens. Sub-bands, which are nominally near the bottom of the well, are therefore pushed up in energy as inter-diffusion increases, while those at the top drop relatively in energy. Conversely, the effect is small in sub-bands near the middle of the QW depth.

The lower energy electrons are strongly confined in the wider well, and the higher energy electrons in both wells. In the "weak coupling" regime, the sub-band spacing increases to a peak shift. At greater inter-diffusion lengths, the sub-band spacing decreases. Inter-diffusion degrades the barrier between wells. Right-bottom inset of Figure 5 shows the "single well" regime, in which large inter-diffusion merges the wells.

Three distinct regimes can be identified, as inter-diffusion increases. For low inter-diffusion the interfaces are almost abrupt, and the barrier is well defined. This effectively uncouples the wells, resulting in very small overlap between the lowest pair of sub-bands. As inter-diffusion increases, the barrier degrades and the wells become weakly coupled, leading to an increased overlap between sub-bands. The bottoms of the wells narrow, leading to increased sub-band spacing. At very large inter-diffusion lengths, the barrier potential is substantially reduced, and the system resembles a single quantum well with the nominal "barrier" region acting as a perturbation. The region of overlap between sub-bands now extends across the entire system, and the energy spacing between sub-bands is determined approximately by the width of the wide, single well and is hence lower than the nominal value. A blue shift in the inter-mini-band emission frequency for GaAs/AlAs superlattices was observed as the inter-diffusion length increased in [59].

3.2. Electric field effect to ADQW states

The resonant situation can be obtained for asymmetric coupled double quantum wells with applied bias [4, 53, 54]. We have performed the same calculations for the diffused ADQW as one of geometry from Figure 4 including the influence of an external electric field E_f. Results were shown at Fig. 6. When an external bias perpendicular to the quantum well is applied, indicated in the Fig. 6 by the changed constant slope, electrons are pushed to one side of the well, thus the effective well width is reduced. At the chosen bias E_f potential tilts downwards from right to left. The middle fan shows how it is possible to change the resonant conditions of longitudinal optical (LO) phonon emission (breaked arrow) to achieve the inversion population at 3rd state for laser effect with FIR

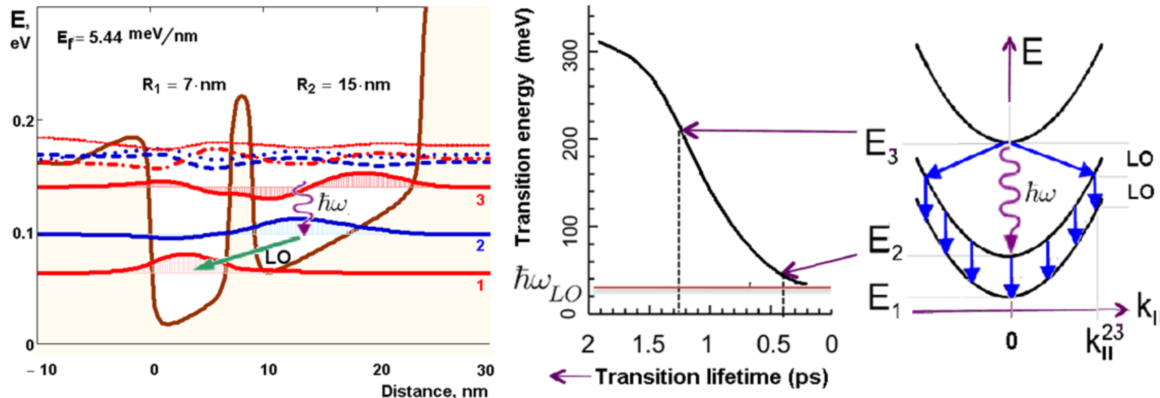

Figure 7. a) Scheme of confined electron states, wavefunctions, and laser transitions at applied external bias 5.44 meV/nm perpendicular to the diffused (Γ = 0.2 nm) ADQW layer plane. (b) The sub-band electron lifetime (inverted horizontal axis) due to optical phonon scattering as a function of inter-sub-band transition energy in a square QW. (c) Engineering a population inversion using the longitudinal optical (LO) phonon resonance. In a ladder of three states, where the two lower ones are spaced by LO-phonon energy, E_3 state's lifetime will naturally be longer than the E_2 because of the smaller ($k^{12} \approx 0$) exchanged wavevector for LO-phonon emission between the 2nd and 1st states. Small vertical arrows show a resonant inter-sub-band LO-phonon scattering. (b,c - adopted from [2])

photon generation (wiggly arrow). Here, once more, we may see an anticrossing situation caused by bias for the levels $n = 0$ and $n = 1$ around the 2-3 meV/nm region of electric field strength.

Investigating structure may work as an electroabsorptive light modulator [17, 18] or as an active stimulated emission region in the far/mid-infrared quantum cascade (QC) lasers [54]. The schematic for this laser operation [4] shown at Fig. 7c is based on a stimulated and cascaded radiative transition from E_3 to a lower sub-band E_2. Depopulation of lower sub-band is achieved by external bias, setting the sub-band separation between levels 2 and 1 to the LO-phonon resonance energy, which causes electrons to quickly relax from level 2 via resonant electron-LO-phonon scattering.

For QC lasers the lifetimes are ultimately limited by LO-phonon emission. The computed [2] inter-sub-band lifetime due to optical phonon emission, is plotted as a function of transition energy for a square QW in Fig. 7b (zero initial kinetic energy in the upper sub-band and zero temperature were assumed). As shown in Fig. 7b, a strong reduction of the lifetime is predicted when the two states are spaced resonantly with the optical phonon energy $\hbar\omega_{LO}$. This increase in scattering rate appears when Δk_{scatt} approaches zero at resonance ($k_{21} = 0$ in Fig. 7c).

A strong reduction of an inter-sub-band lifetime (up to $\approx$ 0.2 ps at Fig 7b) may be obtained by using resonant conditions (electric field tunable) for LO-phonon emission process, when the transition 2→1 approaches the LO-phonon energy value. Consider the structure shown in Fig 7c. In this three-level system, the first two states are separated by optical phonon energy [≈34(36) meV in InGaAs(GaAs)]. Resonant optical phonon emission between these two states will reduce the lifetime of the state $n = 2$ to about $\tau_{21} \approx 250$ fs. LO-phonon scattering is also the dominant non-radiative relaxation mechanism from level 3, but is reduced ($\tau_{32} \approx 1.3$ ps) due to the large in-plane momentum $k_{||}^{23}$ exchange necessary. In other words, 3→2 transitions will proceed with large wavevectors, whereas 2→1 transitions proceed at nearly zero exchanged wavevectors over a whole sub-band (see Fig 7c).

The "resonant-phonon-de-population" design for QCLs was developed in [4, 60]. This design uses combination of resonant tunneling and direct electron-LO-phonon scattering. Electrons are injected by tunneling into the $n = 3$ excited state efficiently filling it. The population inversion (its requirement is simply that $\tau_{32} > \tau_{21}$) is achieved between the two excited states $n = 3$ and 2 (wavy arrow in Fig 7a,c - as 3→2 laser transition). Strong relaxation by emission of optical phonons occurs between the strongly overlapped and closely spaced 2nd and 1st sub-bands.

4. Conclusions

The discreet variable representation approach for solving the Schrodinger equation are performed to calculate the electronic properties of asymmetric double quantum wells with interfaces broadened due to static inter-diffusion effects. Seeking to exploit the inherent flexibility in QW structures, we have presented our results, simulating annealed interfaces with Lorentzian type broadened shapes, as an attempt to model real systems more accurately than

the abrupt rectangular QW approximation. The wave functions and energy states of ADQWs were derived and analyzed in their changes: due to the different mutual widths of coupled wells, for different degree of the broadening, and under increasing external electric field. Our calculations, however, are simulating the behavior of diffused electroabsorptive light modulators [17, 18] and the light-emitter regions of some types of quantum cascade lasers [54].

Perhaps the main conclusion of this work is that the key features for sharp interfaces are preserved, but interface broadening effects change and shift energy levels, but not monotonously. The resonant conditions near the energy of sub-band coupling (anticrossing) regions are not strongly distorted, but anticrossing energy is slightly growing when the interfaces are made smooth. We found, that electric field tunable inter-sub-band energy separations (controlling quantum cascade laser work) were not changed monotonously on the inter-diffusion level, and therefore are important for inter-sub-band optoelectronics technology predictions [2]. It is shown how external bias may help to achieve resonant conditions for inverse population by intra-well emission of LO-phonons.

Acknowledgments

This work was partly supported by the Lithuanian State Science and Studies Foundation grand.

References

[1] K. Talele, E. P. Samuel, D. S. Patil, Optik 122, 626 (2011)
[2] J. Faist, Intersubband optoelectronics (ETH Zurich, Zurich, 2009) www.phys.ethz.ch/~mesoqc/lectures/QCL-lecture-long.pdf
[3] B. Levine, et al., Appl. Phys. Lett. 50, 1092 (1987)
[4] J. Faist et al., Science 264, 553 (1994)
[5] J. Faist et al., Appl. Phys. Lett. 67, 3057 (1995)
[6] A. Valavanis, Z. Ikonic, R. W. Kelsall, Phys. Rev. B 77, 075312 (2008)
[7] T. Sollner, W. Goodhue, P. Tannenwald, C. Parker, Appl. Phys. Lett. 43, 588 (1983)
[8] M. Ghisoni, G. Parry, M. Pate, G. Hill, J. Roberts, Jpn. J. Appl. Phys. 30, L1018 (1991)
[9] W. C. H. Choy, E. H. Li, IEEE J. Quantum Elect. 33, 382 (1997)
[10] I. Gontijo, T. Krauss, R. M. De La Rue, J. S. Roberts, J. H. Marsh, Electron. Lett. 30, 145 (1994)
[11] J. J. He, et al., Electron. Lett. 24, 2094 (1995)
[12] R. Kohler, et al., Nature 417, 156 (2002)
[13] J. S. Yu, A. Evans, J. David, L. Doris, S. Slivken, M. Razeghi, IEEE Photonic. Tech. L. 16, 747 (2004)
[14] J. Zhang et al., Surf. Sci. 600, 2288 (2006)
[15] E. H. Li, B. L. Weiss, K.-S. Chan, IEEE J. Quantum. Elect. 32, 1399 (1996)
[16] W. C. H Choy, E. H. Li, IEEE J. Quantum Elect. 34, 1162 (1998)
[17] E. H. Li, IEEE J. Quantum Elect. 34, 982 (1998)
[18] E. H. Li, IEEE J. Quantum Elect. 34, 1155 (1998)
[19] J. D. Ralston, W. J. Schaff, D. P. Bour, L. F. Eastman, Appl. Phys. Lett. 54, 534 (1988)
[20] J. E. Zucker, et al., Electron. Lett. 28, 853 (1992)
[21] M. Ghisoni, G. Parry, M. Pate, G. Hill, J. Roberts, Jpn. J. Appl. Phys. 30, L1018 (1991)
[22] W. C. H. Choy, E. H. Li, IEEE J. Quantum Elect. 33, 382 (1997)
[23] A. Efros, M. Raikh, In: R. Elliott, I. Ipatova (Eds.), Optical properties of mixed crystals (North-Holland, Amsterdam, 1988) 133
[24] M. Herman, D. Bimberg, J. Christen, J. Appl. Phys. 70, R1 (1991)
[25] E. Runge, Solid State Phys. 57, 149 (2002)
[26] R. Zimmermann, F. Grobe, E. Runge, Pure Appl. Chem. 69, 1179 (1997)
[27] E. Runge, Phys. Status Solidi A 201, 389 (2004)
[28] H. Wang, H. Xu, Y. Zhang, Phys. Lett. A 340, 347 (2005)
[29] V. Gavryushin, SPIE Proc. Ser. 6596, 659619 (2007)
[30] A. K. Ghatak, K. Thyagarajan, M. R. Shenoy, Thin Solid Films 163, 461 (1988)
[31] A. K. Ghatak, K. Thyagarajan, M. R. Shenoy, IEEE J. Quantum Elect. 24, 1524 (1988)
[32] E. Anemogiannis, E. N. Glysis, T. F. Gaylord, T.K. Gaylord, IEEE J. Quantum Elect. 29, 2731 (1993)
[33] E. P. Samuel, D. S. Patil, Progress In Electromagnetics Research Letters 1, 119 (2008)
[34] P. Harrison, Quantum wells, wires and dots: theoretical and computational physics, 2nd edition (Wiley, Chichester, UK, 2005)
[35] B. M. Stupovski, J. V. Crnjanski, D. M. Gvozdic, Comput. Phys. Commun. 182, 289 (2011)
[36] S. F.-P. Paul, H. Fouckhardt, Phys. Lett. A 286, 199 (2001)
[37] K. Nakamura, A. Shimizu, M. Koshiba, K. Hayata, IEEE J. Quantum Elect. 25, 889 (1989)
[38] K. Q. Le, Microw. Opt. Techn. Let. 51, 1 (2009)
[39] D. Colbert, W. Miller, J. Chem. Phys. 96, 1982 (1992)
[40] E. J. Austin, M. Jaros, Phys. Rev. B 31, 5569 (1985)
[41] J. Heremans, D. L. Partin, P. D. Dresselhaus, Appl. Phys. Lett. 48, 644 (1986)
[42] D. Ahn, S. L. Chuang, Appl. Phys. Lett. 49,

1450 (1986)
[43] J. Singh, Appl. Phys. Lett. 48, 434 (1986)
[44] V. Gavryushin, arXiv:q-bio/0510041v1 [q-bio.BM]
[45] E. O. Kane, Phys. Rev. 131, 79 (1963)
[46] J. I. Pankove, Optical processes in semiconductors (Dover Publications Inc., New York, 1975)
[47] E. W. Weisstein, Convolution. Wolfram Web Resource: http://mathworld.wolfram.com/Convolution.html
[48] T. E. Scholesinger, T. Kuech, Appl. Phys. Lett. 49, 519 (1986)
[49] R. Betancourt-Riera, R. Rosas, I. Marin-Enriquez, R. Riera, J. L. Marin, J. Phys. C 17, 4451 (2005)
[50] G. W. Wei, J. Phys. B 33, 343 (2000)
[51] H.S. Lee, J. Light, J. Chem. Phys. 120, 4626 (2004)
[52] J. Tennyson, et al., Comput. Phys. Commun. 163, 85 (2004)
[53] M. A. Stroscio, M. Kisin, G. Belenky, S. Luryi, Appl. Phys. Lett. 75, 3258 (1999)
[54] J. Faist, F. Capasso, C. Sirtori, D. L. Sivco, A. Y. Cho, In: H. C. Liu, F. Capasso (Eds.), Intersubband transitions in quantum wells: physics and device applications, nr. 2, ch. VIII. (Academic Press, New York, 2000)
[55] F. Capasso, et al., J. Quantum Elect. 38, 511 (2002)
[56] J. Faist et al., J. Quantum Elect. 38, 533 (2002)
[57] A. Leuliet et al., Phys. Rev. B 73, 085311 (2006)
[58] F. Stern, S. Das Sarma, Phys. Rev. B 30, 840 (1984)
[59] T. Roch, C. Pugl, A. M. Andrews, W. Schrenk, G. Strasser, J. Phys. D 38, A132 (2005)
[60] B. S. Williams, H. Callebaut, S. Kumar, Q. Hu, J. L. Reno, Appl. Phys. Lett. 82, 1015 (2003)